P5.14 **A SAR-BASED NWP ERROR WARNING PRODUCT**

George S. Young *
The Pennsylvania State University, University Park, Pennsylvania

Nathaniel S. Winstead
The Johns Hopkins University Applied Physics Laboratory, Laurel, Maryland

Todd D. Sikora
Millersville University, Millersville, Pennsylvania

1. INTRODUCTION

Verification of numerical weather prediction (NWP) models at sea is complicated by the relative dearth of in situ observations. Aloft, this issue can be addressed in part by using cloud-track winds. Surface verification is equally challenging, with satellite-borne scatterometers such as ASCAT (Figa-Saldaña et al. 2002) and passive techniques offering the primary means of mapping the oceanic surface wind field (herein, surface refers to 10 m above sea level). In both cases the process is somewhat incestuous as these observations are also assimilated into many over-ocean NWP models. Both also suffer from relatively low spatial resolution, limiting verification of mesoscale and sub-mesoscale features. Spaceborne synthetic aperture radar (SAR) offers the potential to address this resolution issue. SAR also offers the advantage of verifying the NWP model against independent data, unlike scatterometer wind observations which are often assimilated into the model. In this study we used RADARSAT-1 and Envisat Wide Swath synthetic aperture radar (SAR) observations to detect surface wind field errors in the NOGAPS global model. The study focused on the Gulf of Alaska and adjacent waters because of the broad range of meteorological phenomena that inhabit this region.

2. SYNTHETIC APERTURE RADAR WIND

Synthetic aperture radar can be used to estimate the surface wind speed in much the same way scatterometers do, by inverting the radar backscatter from small waves on the ocean surface (Stoffelen and Anderson 1993, 1997). For the SAR wavelengths used in this study, the signal is backscattered primarily by wind-driven waves of a few centimeters wavelength. The inversion is possible because the amplitude of these short waves responds quickly to changes in wind speed (faster winds yield larger wave amplitude), thus changing the SAR backscatter created through a Bragg-like resonance. The relevant wave age is on the order of seconds to 10s of seconds. Thus, fetch is not an issue on large bodies of water. This rapid response, coupled with the high spatial resolution of most satellite-borne SARs, allows for the mapping of surface wind structures at resolutions of 100 m or better.

The diagnosis of surface wind speed from backscatter is usually undertaken using the semi-empirical scatterometer algorithms based on CMOD4 (e.g., Freilich and Dunbar 1999; Stoffelen and Anderson 1993) and CMOD5 (Hersbach 2003). While these algorithms were originally developed for vertically polarized satellite-borne scatterometers, most have been modified for use with horizontally polarized SARs (e.g. Thompson and Beal 2000; Thompson et al. 2001). The results compare well with in situ observations in most cases (e.g., Horstmann et al. 2003; Monaldo et al. 2001, 2004, Fisher et al 2007), although significant errors can result from ocean currents, surfactant slicks, (Johannessen et al. 1999), and non-neutral static stability in the atmospheric surface layer (Foster et al. 2004).

The relationship one inverts to obtain SAR-derived wind speed (SDWS) from SAR backscatter also depends upon the radar look direction relative to the wave crests and thus the surface wind direction. This is because SAR backscatter intensity varies depending on the direction of the incident beam relative to the wave orientation. Thus, wind direction information is required in order to derive surface wind speed from backscatter data. While satellite-born scatterometers such as instrument aboard the ASCAT satellite neatly solve this problem by using multiple look directions, allowing simultaneous diagnosis of both the wind direction and speed, SAR sacrifices that capability as a result of the very antenna configuration and SAR processing that allows it to achieve much higher spatial resolution (Monaldo et al. 2004).

A variety of surface wind direction data have been used in SAR wind speed inversions. Some users deduce the wind direction from the SAR backscatter field itself by observing island wind shadows and boundary layer streaks (e.g. Gerling 1986; Wackermann et al. 1996; Fetterer et al. 1998; Horstmann et al. 2000). Others utilize the course-resolution wind directions available from more-or-less coincident scatterometer observations. In this study we follow Monaldo et al. (2001) in using NWP model fields to provide the wind directions. This procedure offers the operational advantages of global coverage and objectivity. The

* *Corresponding author address:* George S. Young, Dept. of Meteorology, 503 Walker Building, University Park PA, 16802; e-mail: young@meteo.psu.edu

NWP model used for this study was NOGAPS (Monaldo et al. 2001) although others have proved equally appropriate.

3. METHOD

The approach of employing NOGAPS wind directions in the SAR wind speed inversion not only provides guarantee of wind direction data being available, but also allows SAR to be used as a check on model wind direction as well as wind speed. This dual capability arises because there are four possible outcomes of a SDWS-based NWP model wind verification at a given location. First, the SDWS and NWP model surface wind speeds can agree because both the model wind speed and direction are correct. In this situation the SDWS is correct because the NWP model wind direction is correct, and thus the SDWS matches the model wind speed. Second, the SDWS and NWP model wind speeds can disagree because although the model wind direction is correct, and thus the SDWS is correct, the model wind speed is incorrect. Third, the SDWS and NWP model wind speeds can disagree because although the model wind speed is correct, the model wind direction is incorrect, thus the SDWS is incorrect. Unless independent wind directions are available to check against the NWP model wind directions, there is no way to distinguish between the second and third outcomes so as to determine whether it is the model wind speed or model wind direction that is in error. Finally, under fortuitous combinations of NWP model wind speed and wind direction errors, the SDWS may equal the NWP model wind speed. Thus, in this unlikely circumstance, the incorrect SDWS and NWP model wind speeds will match.

4. RESULTS

This procedure for NWP model error analysis was undertaken for 32 cases using SDWS images specifically selected for the mesoscale atmospheric phenomena present, including fronts and their prefrontal jets, gap flows, island wakes, barrier jets, mountain lee waves, and convective outflows (Young et at. 2008). This mesoscale feature-rich sample represents a worse case for the NOGAPS surface wind fields due to their limited spatial resolution. Discussion of the results will begin with detailed analysis of one such case in order to illustrate the consequences of NWP model resolution errors. Discussion of the average error statistics for the full 32 case sample then follows.

4.1 Example case

Figure 1 shows the SDWS image of a portion of a front, marked by the mesoscale transition from postfrontal winds of around 10 m/s to a prefrontal jet of over 20 m/s (Young et al. 2005). The front is progressing northeastward across the image, while the prefrontal jet is blowing from southeast to northwest through the Aleutian Islands. The islands themselves have been masked out in dark blue. Mesoscale

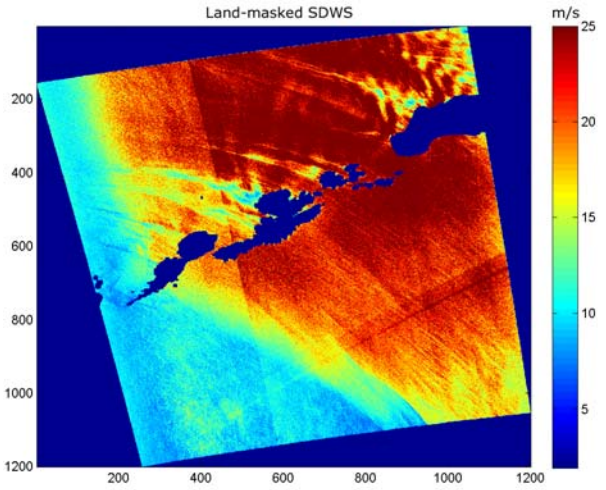

*Figure 1. Portion of a land masked RADARSAT-1 SDWS image of an intense prefrontal low-level jet flowing from southeast to northwest through the Aleutian Islands, 4:46 UTC on February 05, 2007. Image is located near 54 N, 166 W. This image shows the signatures of both island wakes and mountain lee waves. (Provided courtesy of JHUAPL. O*riginal SAR image ©CSA)

features visible in the SDWS image include the signatures of island wakes and mountain lee waves (Schär and Smith 1993). The island wakes appear as bands of lower wind speed in the lee of the islands while the mountain lee waves appear as v-shaped patterns of alternating high and low wind speeds in the lee of the major volcanic peaks of the Aleutian chain.

Figure 2 shows the corresponding NOGAPS

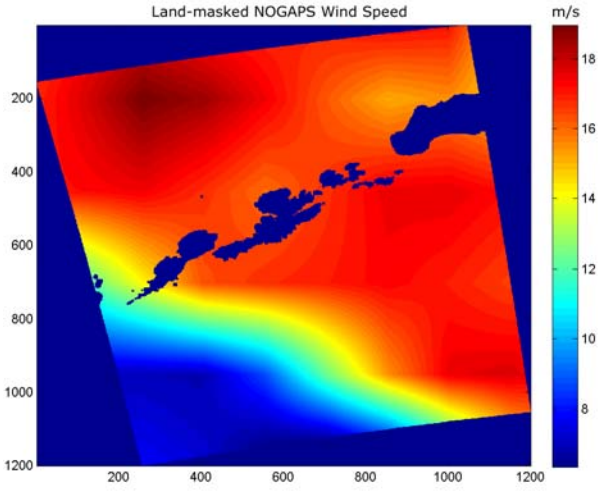

Figure 2. Same as Figure 1, except depicting the corresponding NOGAPS surface wind speed. (Provided courtesy of JHUAPL.)

surface wind speed field. The most striking feature of this field is its relatively low resolution compared with the SDWS image. Despite its inability to resolve

mesoscale flow features, the NOGAPS field clearly captures the sharp wind speed gradient across the front and the intensity of the prefrontal jet.

The difference between the NOGAPS and SDWS fields is thus composed of two components, the fundamental difference on scales resolved by the model (i.e. model error) and the SDWS-detected features at scales not resolved by the model. Figure 3 shows the

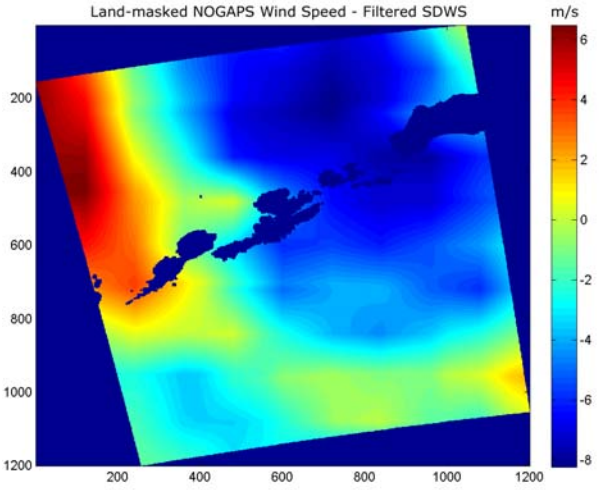

Figure 3. Same as Figure 1, except depicting the difference between the NOGAPS wind speed and the SDWS filtered to the same spatial resolution.

NWP model error on the NOGAPS-resolved scale. While the general depiction of the synoptic situation is good, at least two issues are detected. First, the prefrontal jet is about 4 to 8 m/s slower in NOGAPS than in SDWS. This could be due to either NWP model wind speed error or a difference in wind direction between the model and reality. Given that NOGAPS has the frontal alignment essentially correct, the error is probably primarily in wind speed rather than wind direction.

The second NOGAPS – SDWS difference shown in Figure 3 is the band of positive values along the western edge of the image, particularly north of the Aleutians. This corresponds to a band of anomalously low SDWSs, the result of a lack of dynamic range in the near-range leading to saturation (and hence incorrectly low wind speeds). This example illustrates that one must be careful to distinguish between SDWS errors and NWP model errors as both can be present in the same image.

The second component of wind speed difference field, the SDWS variations on scales too small to be resolved by NOGAPS, is shown in Figure 4. In this image, the signatures of such mesoscale meteorological features as island wakes and mountain lee waves show up clearly, as do beam seams and other SAR processing artifacts. The latter are seen as straight lines or bands across the image. It is noteworthy that the range of wind speed variation is roughly twice as great for this component as for the model error shown in Figure 3. The largest variations occur in the most intense mesoscale flow perturbations: island wakes and

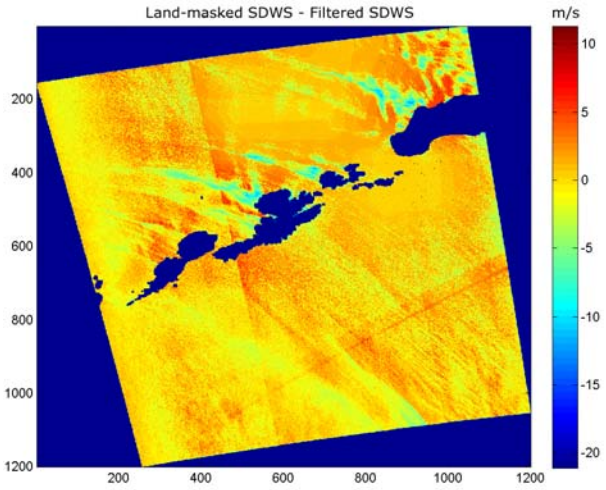

Figure 4. Same as Figure 1, except depicting the SDWS high-pass filtered to eliminate those scales resolved by NOGAPS.

mountain lee waves. Some variation is also evident in mesoscale substructure within the prefrontal jet to the southeast of the Aleutian chain.

Many user communities rely on derived products such as gale warning maps rather than raw wind speed images. Thus, the analysis above is extended to gale warning maps as a means of showing the impact of NWP model resolution, bias, and feature position errors in such products, along with SAR's ability to detect these problems. Figure 5 depicts the SDWS-detected

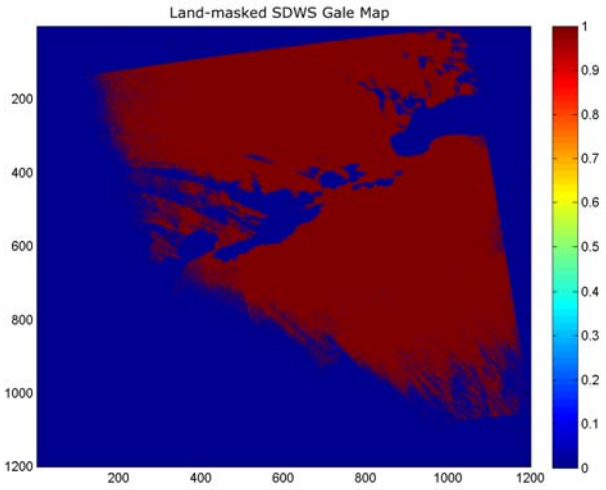

Figure 5. Same as Figure 1, except depicting the coverage of gale-strength winds as detected by SDWS.

gale areas in red. The dominant feature is the band of gales associated with the prefrontal jet. This band is broken by mesoscale lulls associated with island wakes and mountain lee wave crests (i.e. weakened or reversed flow under wave rotors, Vachon et al. 1995, Winstead et al. 2002).

Figure 6 shows how the same gale map would look

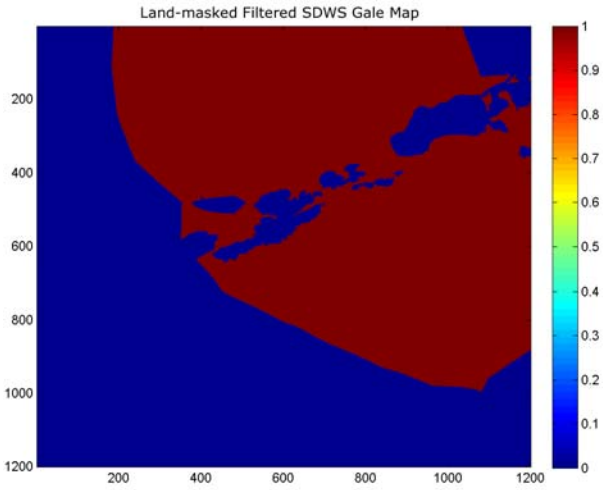

Figure 6. Same as Figure 1, except depicting the coverage of gale-strength winds as detected by the SDWS filtered to the same spatial resolution as NOGAPS.

if the SDWS resolution were reduced to that of NOGAPS. The mesoscale lulls are eliminated while the prefrontal jet gale remains.

Figure 7, shows the corresponding gale map for the

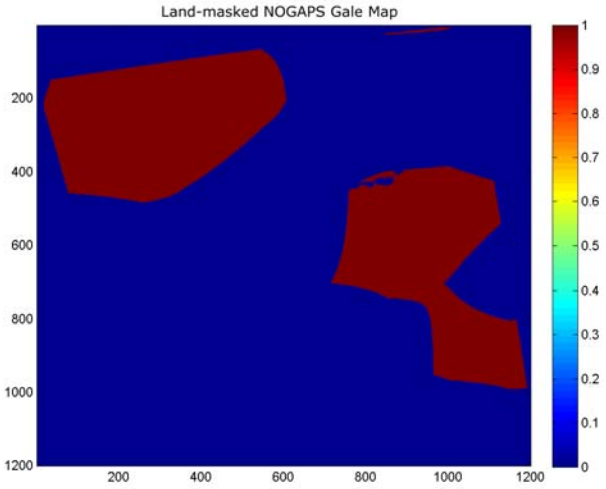

Figure 7. Same as Figure 1, except depicting the coverage of gale strength winds in the corresponding NOGAPS field.

NOGAPS model field. While correctly located, and exhibiting a gap in the lee of the Aleutian chain, the area coverage of gales is much reduced in NOGAPS compared with that seen in Figs 5 and 6. This reflects the speed bias (NOGAPS too slow) noted above, and also suggests that despite its low resolution, NOGAPS is capturing at least the synoptic scale aspects of the mountain-induced decrease in surface wind speed in the immediate lee of the Aleutians.

4.2 Error Statistics

Error statistics were computed and are presented in Tables 1 and 2. Table 1 shows the bias (i.e. the mean difference between NOGAPS and SAR-derived wind speeds), the root-mean squared error (RMSE) between NOGAPS and SAR-derived wind speeds, and the RMSE of the intrinsic SDWS in comparison to that filtered to the NOGAPS resolution. Table 2 shows error statistics for the NOGAPS gale warning map as verified against the corresponding filtered SDWS map. These statistics include threat score (TS), false alarm rate (FAR) and probability of detection (POD) (Wilks, 1995). Both tables include one row for the case discussed above and another for the mean value of each statistic for the set of 32-cases analyzed for this study.

Statistic	Bias (m/s)	RMSE (m/s)	RMSE of unresolved Flow (m/s)
Example	-2.8	4.4	2.1
Typical (32 case sample)	-1.2	3.2	2.0

Table 1. Error statistics for the individual case discussed here and corresponding mean values of these statistics from the 32-case sample analyzed.

Statistic	Gale TS	Gale FAR	Gale POD
Example	0.33	0.21	0.37
Typical (32 case sample)	0.18	0.33	0.21

Table 2. Same as Table 1, except containing the statistics for detection of SDWS-mapped gale-strength winds by NOGAPS. TS is threat score, FAR is false alarm rate and POD is probability of detection.

Table 1 shows that for the set of 32 images, the NOGAPS surface wind speed field shows a slight slow bias, perhaps from its inability to resolve intense mesoscale flows. The RMSE is larger than one would expect from SDWS error alone (Fisher et al., 2007). This undoubtedly reflects the unresolved mesoscale flows as well. Indeed, the RMSE of the unresolved flow is of just about the right magnitude to account for this difference. Taking advantage of the fact that variances sum, one can compute that the RMSE for the resolved scales is about 25% larger than that for the unresolved scales (i.e. 2.5 versus 2.0 m/s).

Table 2 shows that the resolution-induced errors can have a serious impact on NOGAPS gale warning maps. The probability of detection is on average only 21%, indicating that most gale pixels in this SDWS image set are missed by NOGAPS. In contrast, the false alarm rate is only 33%. In combination these statistics indicate that the NOGAPS field is much more likely to miss a gale pixel than to depict one where none exists in the SDWS image. The overall threat score is a relatively poor 0.18.

These results would undoubtedly change, and probably improve markedly, if a high-resolution mesoscale NWP model were verified against the SDWS. The improvement should be particularly good for terrain-driven mesoscale flows where position errors are minimized. In contrast, for mesoscale flows resulting from synoptic scale features, position errors of the parent features could preclude such resolution-based improvement.

5. CONCLUSIONS

SDWS images were analyzed for a number of meteorological phenomena including prefrontal jets, gap flow, island wakes, and mountain waves. The results suggest that NOGAPS surface wind errors result from two primary causes: misplacement of synoptic scale weather features and failure to resolve mesoscale structures of topographic origin. Moreover, verification against SDWSs which have been spatially filtered to the model resolution reveals that RMSE on model resolved scales is typically somewhat larger than that due to the filtering inherent in the model's finite spatial resolution.

Future work should extend this analysis to higher resolution NWP models such as WRF (Schroeder et al., 2006) and to model forecasts as well as analyses.

6. ACKNOWLEDGEMENTS

This work was supported in part by grants ATM-0240869 and ATM-0240269 from the National Science Foundation and grants N00014-10-1-0569, N00014-07-1-0934, N00014-07-1-0577, and N00014-06-1-0046 from the Office of Naval Research.

7. REFERENCES

Fetterer, F., D. Gineris, and C. C. Wackermann, 1998: Validating a scatterometer wind algorithm for ERS-1 SAR. *IEEE Trans. Geosci. and Remote Sensing*, **36**, 479 – 492.

Figa-Saldaña, J., J. J. W. Wilson, E. Attema, R. Gelsthorpe, M. R. Drinkwater, and A. Stoffelen, 2002: The advanced scatterometer (ASCAT) on the meteorological operational (MetOp) platform: A follow on for European wind scatterometers. Can. J. Remote Sens., 28:404–412.

Fisher, C. M., G. S. Young, N. S. Winstead, and J. D. Haqq-Misra, 2007: Comparison of synthetic aperture radar–derived wind speeds with buoy wind speeds along the mountainous Alaskan coast. *J. Appl. Meteor. Climate*, **47**, 1365–1376.

Foster, R., T. D. Sikora, and G. S. Young, 2004: The correction of surface layer wind speeds for atmospheric stratification and height. *Proc. Second Workshop on Coastal and Marine Applications of SAR*, Svalbard, Norway, 2003 September, European Space Agency SP-565, 39-47.

Freilich, M. H. and R. S. Dunbar, 1999: The accuracy of the NSCAT-1 vector winds: Comparisons with National Data Buoy Center buoys. *J. Geophys. Res*., **104**, 11,231–11,246.

Gerling, T., 1986: Structure of the surface wind field from the SEASAT SAR. *J. Geophys. Res*., **91**, 2308-2320.

Hersbach, H., 2003: An improved geophysical model function for ERS C-band scatterometry. ECMWF Technical Memorandum 395.

Horstmann, J., W. Koch, S. Lehner, and R. Tonboe, 2000: Wind retrieval over the ocean using synthetic aperture radar with C-band HH polarization. *IEEE Trans. Geosci. and Remote Sensing*, **38**, 2122 – 2131.

Horstmann, J., J. Schiller, J. Schulz-Stellenfleth, and S. Lehner, 2003: Global wind speed retrieval from SAR. *IEEE Trans. Geosci. Remote Sens*., **41**, 2277 – 2286.

Johannessen, O. M., H. Espedal, B. Furevik, D. Akimov and A. Jenkins, 1999: COAST WATCH: Integrating satellite SAR in an operational system for monitoring coastal currents, wind, Surfactants and oil spills: Proc. Second International Conference on EuroGOOS, Rome, Italy, pp. 11-13.

Monaldo, F. M., D. R. Thompson, R. C. Beal, W. G. Pichel, P. Clemente-Colon, 2001: Comparison of SAR-derived wind speeds with model predictions and ocean buoy measurements. *IEEE Trans. Geosci. Remote Sens.*, **39**, 2587-2600.

_____, D. R. Thompson, W. G. Pichel and P. Clemente-Colón, 2004: A systematic comparison of QuikSCAT and SAR ocean surface speeds. *IEEE Trans. Geosci. Remote Sens.*, **42**, 283-291.

Schär, C., R. B. Smith, 1993: Shallow-water flow past isolated topography. Part I: Vorticity production and wake formation. *J. Atmos. Sci*., **50**, 1373-1400.

Stoffelen, A. and D. L. T. Anderson, 1993: Wind retrieval and ERS-1 scatterometer radar backscatter measurements. *Advance Space Research*, **13**, 53-60.

_____, and _____, 1997: Scatterometer data interpretation: Estimation and validation of the transfer function *CMOD4. J. Geophys. Res.*, **102**, 5767-5780.

Schroeder, A. J., D. R. Stauffer, N. L. Seaman, A. Deng, A. M. Gibbs, G. K. Hunter, and G.S. Young, 2006: An automated high-resolution, rapidly relocatable meteorological nowcasting and prediction system. *Mon. Wea. Rev*., **134**, 1237-1265.

Thompson, D. R. and R. C. Beal, 2000: Mapping high resolution wind fields using synthetic aperture radar. *Johns Hopkins APL Technical Digest*, **21**, 58-67 (Jan-Mar).

Thompson, D. R., F. M. Monaldo, W. G. Pichel, and P. Clemente-Colón, 2001: Combined estimates improve high-resolution coastal wind mapping. *EOS Trans. AGU*, **82**, 469.

Vachon, P. W., Johannessen, J. A., D. P. Browne, 1995: ERS-1 SAR signatures of atmospheric gravity waves. *IEEE Trans. Geosci. Remote Sens*., **33**, 1014-1025.

Wackermann, C. C., C. L. Rufenach, R. A. Schuchman, J. A. Johannesen and K. L. Davidson, 1996: Wind vector retrieval using ERS-1 synthetic aperture radar imagery. *J. Geophys. Res*., **34**, 1343 – 1352.

Wilks, D. S., 1995: *Statistical Methods in the Atmospheric Sciences*. Academic Press, 467 pp.

Winstead, N. S., T. D. Sikora, D. R. Thompson and P. D. Mourad 2002: Direct influence of gravity waves on surface-layer stress during a cold air outbreak, as shown by synthetic aperture radar. *Mon. Wea. Rev*., **130**, 2764-2776.

Young, G. S., T. D. Sikora, and N. S. Winstead, 2005: Use of synthetic aperture radar in fine-scale surface analysis of synoptic-scale fronts at sea. , *Wea. Forecasting*, **20**, 311-327.

Young, G. S., T. D. Sikora, and N.S. Winstead, 2008: Mesoscale near-surface wind speed variability mapping with synthetic aperture radar. *Sensors*, **8**, 7012-7034.